

SPACE SHUTTLE WING LEADING EDGE HEATING  
ENVIRONMENT PREDICTION DERIVED FROM  
DEVELOPMENT FLIGHT DATA

John A. Cunningham  
Joseph W. Haney, Jr.  
Space Transportation and Systems Group  
Rockwell International  
Downey, California

SUMMARY

An analytical program is in progress at Rockwell International to revise wing leading edge heating predictions in order to improve correlation with STS-1 to -5 flight thermometer data. This paper discusses the methods that have been used to improve agreement between prediction and flight and summarizes the aerothermodynamic correlations which, when updated, will be used to analyze future orbiter missions.

INTRODUCTION

The first two phases of the project Columbia (OV-102) orbiter STS-1 through STS-4, were dedicated to obtaining engineering flight data for system verification that would lead to operational verification of OV-102 and subsequent orbiters. Later in the project it was decided to record Development Flight Instrumentation (DFI) during the first operational mission. Since the STS-1 mission fell within the OFT entry envelope, these data have also been included in this study. Prior to STS-1, extensive DFI were defined, designed, and installed on the vehicle. Some of the sensors, such as thermocouples, pressure taps, and associated electronic components, were off-the-shelf items. Others, because of sensitivity or accuracy requirements, flight environment exposure, etc., were designed and fabricated by Rockwell International.

It is necessary to design all DFI so that the function of the component or subsystem parameter measured was not degraded. Because of the Thermal Protection System (TPS) criticality and susceptibility to damage during liftoff acoustics and flight airloads, TPS sensors frequently required a unique engineering approach and, in some cases, ground testing to test sensor function and to insure that the component or subsystem integrity was not impaired.

Wing leading edge heating data were required during the Orbiter Flight Test (OFT) program to validate the technical prediction methods used prior to STS-1 and to provide flight data to modify these methods if necessary. Leading edge data were particularly important because of the uncertainties in scaling from wind tunnel to flight conditions. Standard aerothermodynamic equations fitted to include wind tunnel derived constants have been used to make the initial environment predictions prior to STS-1.

An engineering study of leading edge measurement methods was performed. It was concluded that use of thermocouples to measure the panel inner mold line (IML) temperature would be highly undesirable. It was recommended that a pyrometric device, later termed a radiometer, should be mounted on the leading edge spar and focused on the RCC panel inner mold line (IML) to measure IML temperature.

#### SYMBOLS

$\alpha$	angle of attack
$\gamma$	specific heat ratio
$\Delta$	leading edge sweep, geometric
$\Delta_{EFF}$	effective leading edge sweep
$q_{LE}$	heat rate of leading edge stagnation line
$q_{1'R}$	heat rate to a one foot radius sphere
$R$	leading edge radius
$R_{EFF}$	effective leading edge radius
$R_{ACT}$	actual leading edge radius
$C_p$	local pressure coefficient
$C_{ps}$	stagnation pressure coefficient
$V_\infty$	freestream velocity
$f$	heat flux scale factor
$q'$	assumed surface heat flux
$q_{REF}$	preflight surface heat flux

This paper compares typical data obtained during the first five flights, which included the OFT Program STS-1 to -4, to preflight predictions. Using radiometer data, a method was developed to adjust the heat flux levels and leading edge heating distribution to improve agreement between the predictions and radiometer flight data. This was accomplished by performing parametric thermal analyses at RCC panels 9 and 16 thereby establishing the required scaling necessary to insure agreement. The effect of scaling on internal insulation and leading edge spar predicted temperatures was compared to flight data at panel 9 and an investigation performed using other panel 9 OFI to explain what at first appeared to be differences between temperatures predicted using these RCC heating corrections and flight temperatures.

## SYSTEM DESCRIPTION

The orbiter wing leading edge is a subsystem of the Thermal Protection System that has been designed to withstand entry heating for as many as 100 Shuttle missions. The leading edge consists of 44 reinforced carbon-carbon (RCC) wing panels, 22 panels per wing (fig. 1). Left-hand and right-hand wing panels are mirror images; however the molded, high-temperature processes used during fabrication require individual panel designs and fabrication tooling.

An RCC T-seal that serves as an aerodynamic transition between adjacent panels is mechanically assembled to the outboard surface of each panel. The T-seal functions primarily as an expansion joint which is designed and fitted to inboard and outboard mating panels. The T-seal prevents boundary layer plasma flow from the windward, high pressure surface into the reduced-pressure internal cavity during entry. Figure 2 is an exploded view of the panel showing the panel assembly of a typical panel/T-seal set and the attachment arrangement for OV-102.

Nickel alloy fittings fasten each panel at two inboard and two outboard locations called field breaks by means of brackets mounted from the wing box forward spar. This arrangement allows easy assembly of the panel to the forward spar and permits removal of panels either singly or in groups. The fittings are shimmed to allow adjustment of the panel, thereby insuring proper alignment and fitup. Cross sections through the panel attachment plane and mid-panel shown on figure 3 provide the attachment arrangement and the other major subsystem assemblies, the spar insulation, and upper and lower access panels.

A spar insulation blanket protects the aluminum wing box structure from the intense radiant heating environment of the RCC cavity during entry ( $T_{max} = 2600^{\circ}F$ ). Access panels, as the name implies, provide access to the leading edge cavity to perform inspections with the wing panel on the vehicle and also permit access to the field break bolts for panel removal.

## LEADING EDGE INSTRUMENTATION

Early in the Shuttle program, a study was performed to determine possible ways of measuring the entry heat rate to the RCC. One method that would use conventional calorimeters was ruled out because of the extreme thermal environment. A second method considered provided for bonding high-temperature thermocouples (T/C) to the RCC inner mold line. After a critical evaluation of a T/C application, use of thermocouples was discarded for the following reasons.

- The influence of the T/C on RCC panel structural integrity would be very difficult to assess.
- A high-temperature T/C installation required ceramic bonding that would be highly susceptible to failure during the liftoff acoustic environment.

- Thermal ground test experience showed that the T/C junction would rapidly degrade. This degradation occurs at flight temperature levels as a result of T/C junction deterioration in the presence of silicon carbide, the RCC panel coating material.

The only acceptable alternate proved to be a noncontact temperature-measuring device that operates similar to a pyrometer. This device, which was termed a radiometer, could be calibrated to continuously measure RCC panel IML temperatures during the entry.

The radiometer is a thermoelectric device that functions in conjunction with a lens system that collimates incident thermal energy to a thermopile sensor. The sensor millivolt output is calibrated as a known function of source temperature and emittance and, in operation, provides a continuous readout of RCC temperature. The sensor/lens configuration was mounted in a thick-walled copper shroud that had been designed to maintain the radiometer temperature at acceptable levels. Figure 4 shows the assembled radiometer.

Five leading edge radiometers were installed in the OV-102 L/H leading edge to measure RCC temperature in two ranges: 302°F to 2570°F and 410°F to 3000°F. These two ranges were selected by considering the predicted flight temperatures and the desire to achieve maximum accuracy within each range.

The leading edge radiometer installation had to be maintained in a thermal environment that would not exceed its operating temperature range of -250°F to 600°F. This was accomplished by imbedding each device in a 22 PCF (LI 2200) RSI tile which, in turn, was recessed in the Inconel-Dynaflex spar insulation panel. The OV-102 type installation at panel 16 L/H is shown in figure 5.

Five radiometers were installed in four OV-102 L/H wing panels as shown on figure 6. Four of these were selected to measure maximum heating region temperatures at panels 4, 9, 16 and 22. The fifth measured panel 9 leeward surface data so that data at two locations would be available to infer heat flux distribution at panel 9. Table I summarizes the radiometer location plan, identifies sensor number (V09T9909A, etc.), and denotes sensor function.

## PREFLIGHT ANALYSIS METHODS

### Aerothermodynamic Methods

The wing leading edge of the Shuttle orbiter was aerothermodynamically modeled by first simplifying the design into its basic shape, a swept cylinder. Using this approach the leading edge consisted of a 45-degree swept cylinder with regions of higher sweep at the glove fillet and at the wing tip.

Using this simplified geometric approach allowed the use of the swept cylinder equation:

ORIGINAL PAGE IS  
OF POOR QUALITY

$$q_{LE/q} = \frac{1}{\sqrt{2}} \cdot \sqrt{\frac{1}{R}} \cos^{1.2} \Lambda_{EFF}$$

where

$$\Lambda_{EFF} = \sin^{-1}(\cos \alpha \cdot \sin \Lambda)$$

C  
.. In reality, the treatment of the leading edge as a cylinder was only applicable at the forwardmost region, since the cylinder region was blended into airfoil sections forming the wing. To account for this change to the leading edge shock shape, wind tunnel test data were correlated to determine the relationship between the actual geometric radius and the effective radius that influences heating. This analysis resulted in the following relationship:

$$\Lambda_R = R_{EFF} = \left( \frac{R_{EFF}}{R_{ACT}} \right) \cdot R_{ACT}$$

where

$$\frac{R_{EFF}}{R_{ACT}} = \text{EXP} \left[ f(\alpha) - \cos^{1.3} \Lambda \right]$$

and where

$$f(\alpha) = .18513 - .0240167\alpha + .00280425\alpha^2 - .000024\alpha^3$$

In computing pressure, a simplified approach was again taken to determine the pressure along the stagnation line of the leading edge, so that

$$C_p/C_{PS_{max}} = \cos^2 \Lambda_{EFF}$$

These two approaches were taken to define the environments to the stagnation line of the leading edge away from regions of disturbance (bow shock impingement). This approach was validated through wind tunnel test data.

To transfer from the stagnation line on the LCC to the closeout HRSI tiles on the wing upper and lower surface, a modified Beckwith and Cohen distribution (ref. 1) was utilized to allow for a smooth variation between leading edge and wing.

The prior discussion pertains only to the regions of the wing leading edge outside of the bow shock-leading edge shock interaction (i.e., greater than 55 percent semispan).

Analysis of schlieren data, oil flow patterns, and heat transfer data from wind tunnel tests indicated that the bow and leading edge shock impinged with a resulting third shock and vortex/jet impinging on the wing. The shock pattern was similar to the type V pattern of Edney (ref. 2). The main effects of this disturbance were increased heating at 55 percent semispan on the leading edge, earlier transition on the outboard portions of the wing lower surface, and vortex scrubbing on the outboard wing upper surface.

By using heat transfer data obtained from thin film gage wind tunnel tests and the previously mentioned swept cylinder approach, the effects of shock impingement during wind tunnel conditions were determined.

The importance of scaling the effects of shock impingement from wind tunnel to flight conditions was indicated by the work of Edney and Keyes and Hains (ref. 2 and 3) relative to  $\gamma$ . These works showed that the theoretical calculation of the inviscid shock interaction flow field in connection with empirically derived correlations of the viscous interaction phenomenon caused the interaction to be more severe as the specific heat ratio decreased. Additional analysis by Bertin et al. (ref. 4 and 5) related the pressure changes across the "double-shock" system to shock pattern changes and thereby heat transfer with freestream velocity. These analyses were used to develop a scaling correlation from wind tunnel measured data to anticipated flight conditions.

In addition to scaling the magnitude of the shock impingement heating, the location of the shock interaction as it traveled along the leading edge was correlated with  $\gamma$  and  $V_\infty$  and allowed to vary throughout reentry.

The combined effects of scaling the wind tunnel data to flight using the double-shock and traveling-shock procedures resulted in maintaining the maximum level of heating as indicated by direct scaling of the wind tunnel data but moved the peak heating location inboard of the wind tunnel impingement location.

#### Thermal Analysis Methods

The leading edge radiometers measured RCC IML temperatures directly, and these temperatures could be rapidly compared to OFT preflight IML temperature predictions. However, the primary purpose of the radiometers was to provide temperature data that would be used to calculate OML heat rate histories and heating distributions experienced by the RCC surface during entry. The conversion of IML temperature data to OML heat flux predictions required a detailed thermal analysis of the radiation enclosure formed by the leading edge cavity that consists of the panel IML and the spar insulation surface.

Two dimensional thermal math models (TMM) were developed to convert radiometer temperatures to surface heating. The TMM for panel 16 is shown on figure 7. Except for panel geometry, a second model developed for panel 9 is thermally identical to the panel 16 model. As flight data became available, these models were used to perform analyses using data from the panel 9 radiometers V09T9926A and V09T9927A and the panel 16 radiometer V09T9934A (see table I).

The panel 9 and 16 locations were selected for flight data analyses since panel 9 is in the peak entry heating zone and panel 16 is in the maximum entry airload zone. These two locations are the most critical of the leading edge subsystem. The panel 4 glove and panel 22 wing tip radiometer data are in much less severe heating environments; however, radiometer data at these locations were useful to compare directly to predictions and provided the means to establish temperature/heating trends at these locations. If flight data warranted study at the glove and wing tip environment in greater detail, analyses similar to the panel 9 and 16 data analyses could be performed to establish heat rates at these locations. After examining entry flight data, to conserve time, it was decided to use approximate methods of calculating heat flux at this time since, as will be shown in the next section, the data at these two wing zones were indeed thermally less critical.

## OFT FLIGHT DATA

### Entry Trajectory Definition

The development flight test program consisted of four orbital missions, STS-1 through STS-4, with launch inclinations varying from 28.5 degrees to 30.5 degrees. All four entry trajectories were quite similar, with the majority of each entry having the orbiter attitude at an angle of attack of 40 degrees to the velocity vector. STS-3 and STS-4 differed slightly from the first two flights in that the flying time was approximately 100 seconds shorter for each flight. As previously noted, DFI were also recorded during the STS-5 first operational mission, and these data have also been included in this study.

### Flight Data Overview

Unfortunately, because of a malfunction of the orbiter flight recorder during STS-1 and STS-4, only telemetered down-link data were recorded. Since down-link data can only be transmitted after the blackout period (approximately 950 seconds) while the peak heating plateau extends from 350 to 800 seconds, peak heating data were not available for these flights. Fortunately, however, this problem was avoided during STS-2, -3 and -5 so that a full complement of DFI including leading edge radiometer data was obtained during these flights.

Maximum heating radiometer data from STS-1 and STS-2 are compared to the pre-flight prediction for panel 9 (V09T9926A), 55 percent semispan, on figure 8 and for panel 16 (V09T9934A), 80 percent semispan, on figure 9. The predicted temperature is seen to be several hundred degrees lower than flight data at panel 9 while data and prediction are in excellent agreement at panel 16. From these comparisons, it could be concluded that predictions using the swept cylinder approach with modifications based on wind tunnel data, such as the panel 16 analysis, were generally validated by flight data. However, at panel 9, which is in the 45 percent to 55 percent semispan bow shock interaction region, the predictions are low. Inspection of the temperature distribution provided by the panel 9 leeward radiometer (V09T9927A) plotted on figure 10 further substantiates this trend.

ORIGINAL PAGE IS  
OF POOR QUALITY

Panel 4 (40 percent semispan) and panel 22 (98.6 percent semispan) maximum heating radiometer data were compared to prediction by first calculating the surface heat rates at these locations. This comparison was completed for the remainder of the wing by performing similar calculations at panel 9 and panel 16. Maximum heating was then plotted as a function of percent semispan on figure 11. Both the panels 4 and 22 heat rates in the glove and wing tip are substantially overpredicted, as had been expected since the swept cylinder approach is known to be conservative in regions of high sweep.

#### TECHNICAL DISCUSSION

The five radiometers in the leading edge provided the temperature data that were required to establish leading edge heating. To facilitate analyses, the leading edge was partitioned into three heating zones: 45 degrees swept wing, bow shock impingement or double shock zone, and highly swept wing, which consisted of the wing glove and wing tip. The bow shock impingement zone, panel 9, was of particular interest since it was in the maximum heating zone.

Two of the five radiometers were installed at panel 9. The first radiometer (V09T9926A) monitored peak heating temperature and the second (V09T9927A) was focused on the leeward wing surface. It had been planned to use the data from these two instruments in combination to determine both heat flux level and heat flux distribution for the panel. Other radiometer locations were the highly swept wing glove panel 4 (V09T9909A), the wing tip panel 22 (V09T9940A), and the 45 degree swept wing outboard of the double shock zone at panel 16 (V09T9934A).

The panel 9 peak heating region and panel 16 maximum ascent/entry airload location were selected for study because they are critical to the thermal and structural evaluation of the leading edge subsystem. It was for this reason that math models had been developed to analyze these locations.

Revision of wing heating methods would be as accomplished in two steps.

1. Thermal math models would be used to perform parametric analyses to establish heating levels and heat flux distributions and to improve agreement between RCC predictions and flight data.
2. The amended heating would then be used as the basis to revise aerothermo correlations used to predict leading edge heating rates. These revised correlations would then be employed to perform aerothermo analyses for ETR missions and might also be used to estimate heating for other missions such as WTR missions.

Other DFI that provided spar insulation surface temperature, spar temperature, and attachment temperatures were also used to validate the heating update.

## Double Shock Region Analyses

The peak windward heating and leeward radiometer data for panel 9 were compared to predictions on figure 10. This comparison indicated that preflight STS-1 heating methods used to predict RCC temperatures provided the proper heating trend; however, they underpredicted the flight data by approximately 200°F. As a first attempt at correlation, parametric analyses were performed in which heating values were parametrically increased by a multiplier. The multiplying factor  $f$  was defined as

$$f = \frac{q'}{q_{REF}}$$

where

$$q = q(\theta, T_w, S)$$

and

$\theta$  = Time from entry interface, seconds

$T_w$  = Surface temperature, °F

$S$  = Surface location, inch

RCC temperature was then plotted as a function of the multiplier ( $f$ ) to compare with flight data.

These curves for both peak heating (V09T9926A) and leeward (V09T9927A) radiometers are plotted on figures 12 and 13. Both plots were found to be linear and indicate peak temperatures from STS-2, -3, and -5 radiometer data can be correlated with a scale factor of 1.32 to 1.37 for both maximum heating and leeward radiometers. A factor of 1.34 was selected to best represent the flight data range for both radiometers.

At this time, another panel 9 shell analysis was performed using STS-1 preflight heating with a multiplier of 1.34. The results of this analysis are compared to flight peak temperature data in table II and on figures 14 and 15.

Table II summarizes RCC panel peak temperature predictions and shows that the scaled surface heating ( $f = 1.34$ ) provides virtual agreement between predicted and flight maximum temperatures. A more critical comparison is shown by figures 14 and 15, in which radiometer temperature-time data are compared to the revised predictions. The curves show that the correlation between predicted RCC temperature and radiometer data is substantially improved when the 1.34 factor is applied. Radiometer data could not be plotted below the sensor threshold temperature, 500°F on the figures. Correlation with internal temperature measurements, consisting of three insulation surface thermocouples and two structural forward spar measurements, is summarized in table III and figures 16 through 18.

The peak insulation temperatures in table III are seen to exceed flight data, which seems to contradict the requirement to increase surface heating to correlate RCC temperature. After studying the other DFI data at panel 9, a reasonable explanation for this deviation was reached. This explanation is best understood by first examining flight data obtained at the panel 9 outboard attachment, rib station 10.

Analytical predictions for the RS10 panel clevis and spar are compared to STS-2 flight data on figures 19 and 20 respectively. The accuracy of the RS10 attachment math model used for the predictions had been verified with full-scale ground test data obtained at the NASA Johnson Space Center Radiant Heating Test Facility early in the program so that there was a high confidence level in the capability of the models to accurately predict attachment temperatures. However, the test correlation had been performed for a purely conduction/radiation test environment. Removal of leading edge panel 9 after the OFT flights had shown that high-energy air was leaking past the lower access panel thermal barriers into the RCC cavity from the windward surface. High-temperature gas streaks were evident both on the aluminum spar and on the lower spar bracket and the lower attachment clevis. Since the attachment model had been "tuned" to a radiant heating ground test, which did not simulate boundary layer heating or the surface pressure gradients that would lead to gas in-flow and gas streaking that occur during flight, internal convection not included in preflight analyses would be a potential source of deviation between prediction and flight.

In fact, it was concluded that this was the case, and inspection of the panel clevis and spar bracket flight temperature traces for STS-2 clearly show that convection strongly influenced these temperatures. This is most clearly shown on figure 20 by the rapid rise of the spar bracket temperature (V09T9911A) at RS10 that can only be heat transfer from initially hot gas in-flow followed by a spike and rapid reduction that would indicate a reduced inflow gas temperature and bracket cooling. The subsequent reversal and increase of the bracket temperature after touchdown is most likely due to residual heat transfer from the aluminum wing box. Convection is also felt to be present with the panel clevis (V09T9919A) whose temperature is plotted on figure 19. The latter figure indicates that air in-flow produces a net cooling of the clevis.

From the foregoing flight data and consideration of the spanwise pressure gradients in the leading edge, it was further concluded that air flow and convection do occur in the OV-102 leading edge cavity and, therefore, convection may affect the temperatures of subsystem components in the cavity. It is likely, therefore, that spanwise air currents will occur as well as local inflow from the windward high-pressure surface.

With convection present in the panel 9 cavity, it is reasonable to assume that air convection, not accounted for in the insulation temperature predictions, may account for the difference observed between the predicted insulation temperature and flight data shown on figures 16 through 18. In this case, the consistently lower insulation flight temperatures indicate that there is a net cooling of the insulation surface.

Table III shows that the model gives a reasonable correlation of spar average temperature that adds additional confidence to use of surface heating factors to simulate soakback heat loads to the spar. It should be emphasized, however, that the complex construction and heating environment of the wing box are not adequately modeled in the panel 9 TMM and that the spar temperature prediction is considered only an approximation.

#### 45 Degree Swept Wing Analyses

The logic used to develop the surface heating factor for panel 9 was extended to panel 16, which is outside of the wing zone affected by bow shock impingement. Although only a single radiometer (V09T9934A) was located at panel 16, panel 9 data indicated it was reasonable to assume that temperature/heating distributions are the same as predictions.

Comparison of STS-2 radiometer data to the preflight prediction in figure 9 showed excellent agreement, and only minor deviations from preflight predictions were evident. The panel 16 radiometer parameter study (figure 21) showed that heat flux required to correlate flight data was with 2 percent of the preflight prediction. This is considered to verify swept-wing methods outside of the shock interaction zone and no scaling (i.e.,  $f = 1.0$ ) would be required in this wing zone. The maximum temperatures predicted using preflight heating ( $f = 1.0$ ) are compared to flight data in table IV. Unfortunately, the single insulation surface thermocouple V09T9931A had been lost prior to STS-1 so that a comparison of insulation flight data at panel 16 was not possible.

#### Highly Swept Wing Analyses

Both panel 4 wing glove radiometer data (V09T9909A) and panel 22 wing tip data (V09T9940A) indicated heat flux levels substantially lower than predicted (see fig. 11). The comparison of temperature history data to flight data plotted on figures 22 and 23 showed that this was true at panel 4 but not true at panel 22 for the following reason. The panel 4 plot on figure 22 clearly shows a peak temperature overprediction of 260°F while the panel 22 prediction is in excellent agreement with data until 900 seconds. At that time, the onset of boundary layer transition that was assumed in the prediction causes a predicted temperature excursion which really doesn't occur in flight. Accordingly, it was concluded that the existing wing tip analysis method is adequate to predict flight heating provided transition is ignored.

#### Analyses Summary

The results of the foregoing discussion are summarized in table V, which provides temperature comparisons between flight and prediction and scale factors  $f$  that, when applied to preflight aerothermo analyses, will improve heating/temperature predictions at the three wing leading edge heating zones considered.

## CONCLUDING REMARKS

Leading edge panel thermal math models have been developed and used to establish scale factors that, when used in conjunction with preflight heating, improve the correlation with flight radiometer data. These factors may be used to perform leading edge analyses for the 45-degree swept wing zone, double-shock region, and the two highly swept wing zones. Data from other DFI at panel 9 generally corroborate the revised surface heating approach; however, there is evidence that RCC cavity air convection influences subsystem internal component temperatures. This source of heat transfer is not fully understood at this time and could not be included in this study.

This leading edge heating update will form the basis for revision of aerothermo analysis methods used to predict the leading edge heating environments. These revised methods can then be used to analyze future ETR missions and to estimate environments for other orbiter missions.

## REFERENCES

1. Beckwith, J. E., and Cohen, N. B., Application of Similar Solutions to Calculation of Laminar Heat Transfer on Bodies with Yaw and Large Pressure Gradients in High Speed Flow, NASA TN D-625, January 1961.
2. Edney, B., Anomalous Heat Transfer and Pressure Distribution on Blunt Bodies at Hypersonic Speeds in the Presence of an Impinging Shock, Aeronautical Research Institute of Sweden, FFA Report 115, February 1968.
3. Keyes, J. Wayne and Hains, Frank D., Analytical and Experimental Studies of Shock Interference Heating in Hypersonic Flows, NASA TN D-7139, May 1973.
4. Bertin, John J., Graumann, Bruce W., and Goodrich, Winston D., High Velocity and Real-Gas Effects on Weak Two-Dimensional Shock Interaction Patterns, J. Spacecraft, Vol. 12, No. 3, March 1975.
5. Bertin, John J., Mosso, Stewart J., Bacrette, Daniel J., and Goodrich, Winston D., Engineering Flowfields and Heating Rates for Highly Swept Wind Leading Edges, J. Spacecraft, Vol. 13, No. 9, September 1976.

TABLE I.-OV-102 WING LEADING EDGE RADIOMETERS

Percent Semispan	Panel	Sensor V09TXXXXA	Range, °F	Surface Measured	
				Maximum Heating	Leeward
40	4	9909	410-3000	X	
55	9	9926	410-3000	X	
55	9	9927	302-2570		X
80	16	9934	410-3000	X	
98.6	22	9940	410-3000	X	

TABLE II.-PANEL 9 RCC FLIGHT DATA CORRELATION

RCC IML Location	Sensor V091XXXXA	Maximum Temperature, °F		
		Flight	f= 1.0	f= 1.34
Maximum heating	9926	2490	2262	2475
Leeward	9927	1910	1735	1920

TABLE III.-PANEL 9 INSULATION/SPAR FLIGHT DATA CORRELATION

Component	Sensor V09TXXXXA	Maximum Temperature		
		Flight	f= 1.0	f = 1.34
Insulation				
Lower surface	9922	2010	1986	2180
Center	9918	1835	1930	2100
Upper surface	9923	1750	1860	2040
Spar				
Lower spar cap	9915	290	229	280
Upper spar cap	9911	210	210	250
Average	-	250	220	265

TABLE IV.-PANEL 16 FLIGHT DATA CORRELATION

Component	Sensor V09TXXXXA	Maximum Temperature, °F	
		Flight	f= 1.0
RCC, max heating	9934	2110	2086
Insulation center	9931	—*	1849
Lower spar	9929	248	175
*Data questionable for STS-1 through STS-5			

TABLE V.-WING LEADING EDGE RECOMMENDED SCALE FACTORS

Panel	Semispan	Radiometer V09TXXXXA	RCC Maximum Temperature, °F			Recommended Scale Factor, f*
			Preflight	Radiometer	Revised	
4	40%	9909	2070	1800	1800	0.48
9	55%	9926	2260	2480	2500	1.34
9	55%	9927	1760	1910	1925	1.34
16	80%	9934	2100	2110	2100	1.8
22	98.6%	9940	2050	1835	1800	1.9

Note: All temperature are RCC inner mold line

$$*f = \frac{q'}{q_{REF}}$$

$$q = q(\theta, T_w, S)$$

ORIGINAL PAGE IS  
OF POOR QUALITY

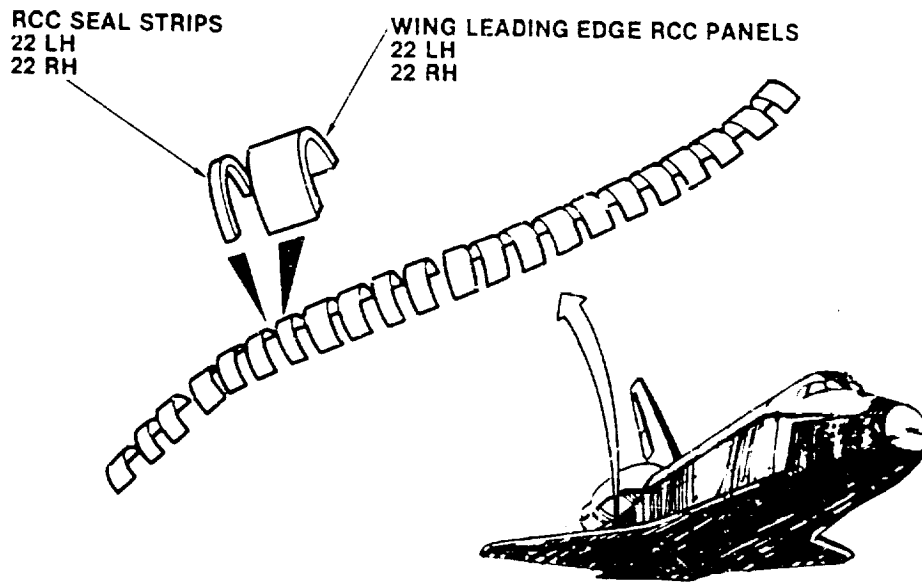
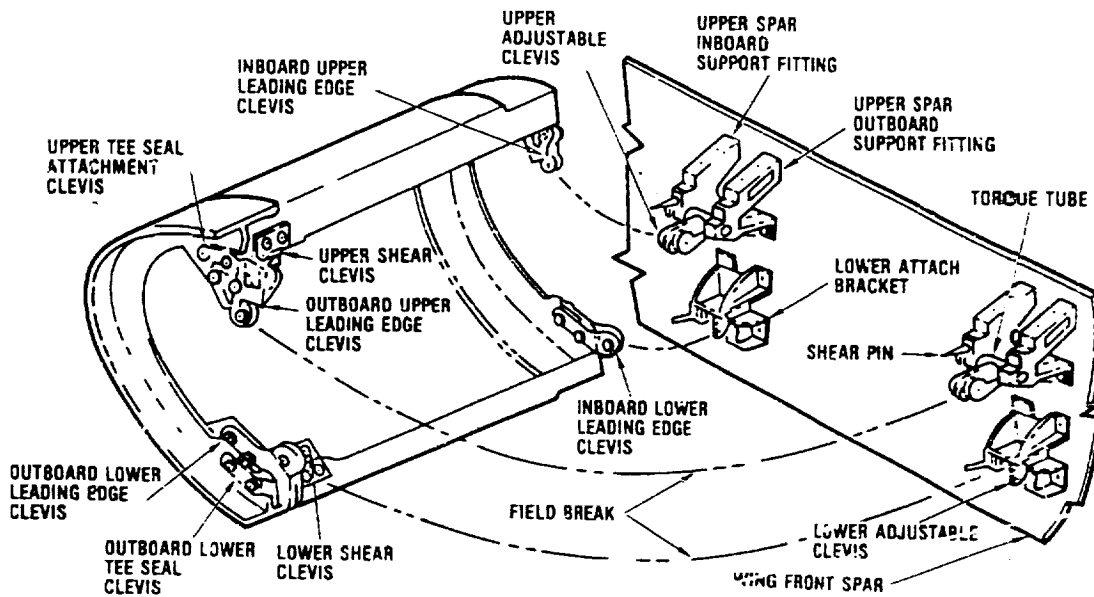


Figure 1.- Shuttle orbiter wing leading edge configuration.



NOTE:  
WING SPAR AND ATTACHMENT INSULATION  
HAVE BEEN OMITTED FOR CLARITY

Figure 2.- Leading edge attachment arrangement.

ORIGINAL PAGE IS  
OF POOR QUALITY

MIDPANEL SECTION

END SECTION

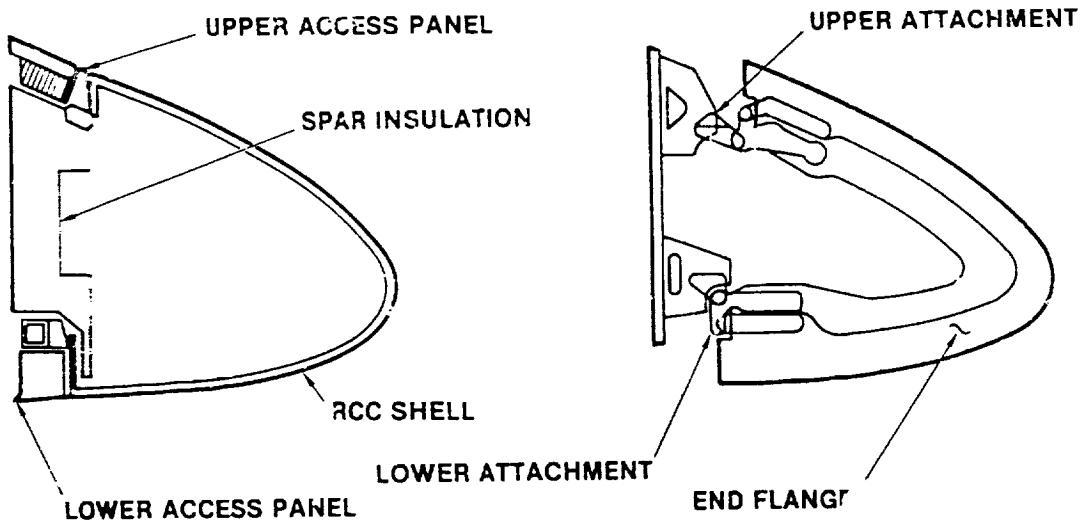


Figure 3.- Leading edge panel shell and end flange sections.

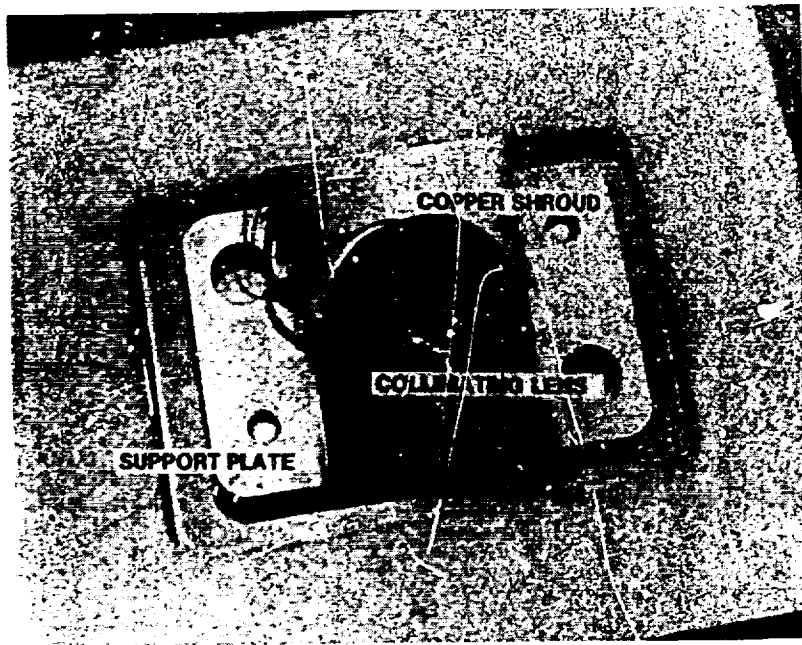


Figure 4.- Radiometer assembly.

ORIGINAL PAGE IS  
OF POOR QUALITY

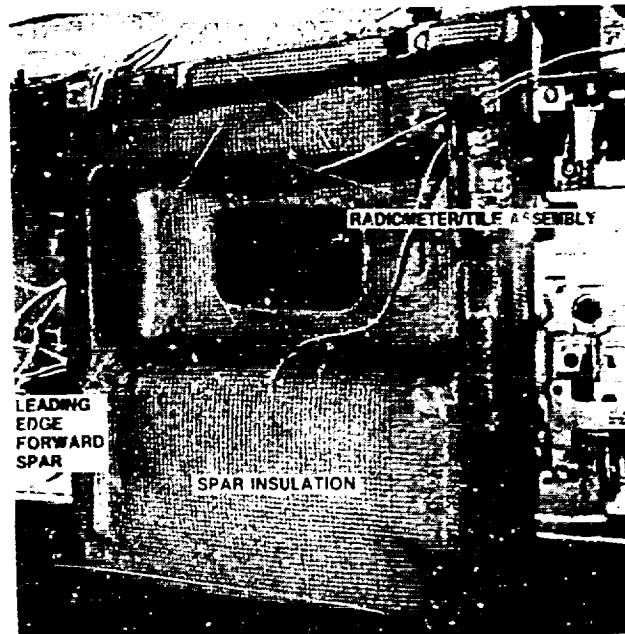


Figure 5.- Panel 16 radiometer installation.

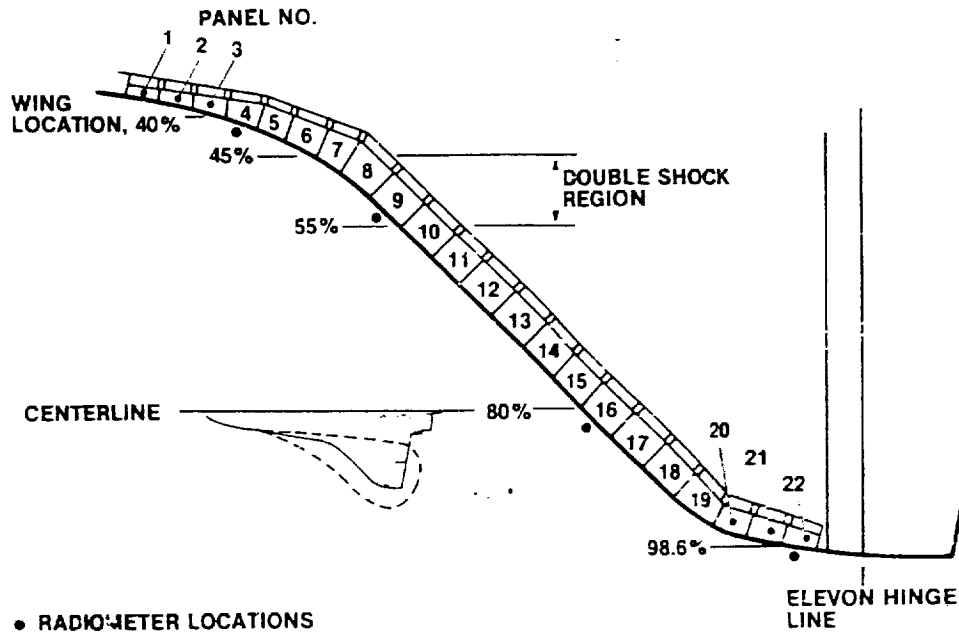


Figure 6.- Orbiter vehicle 102 radiometer locations.

ORIGINAL PAGE 13  
OF POOR QUALITY

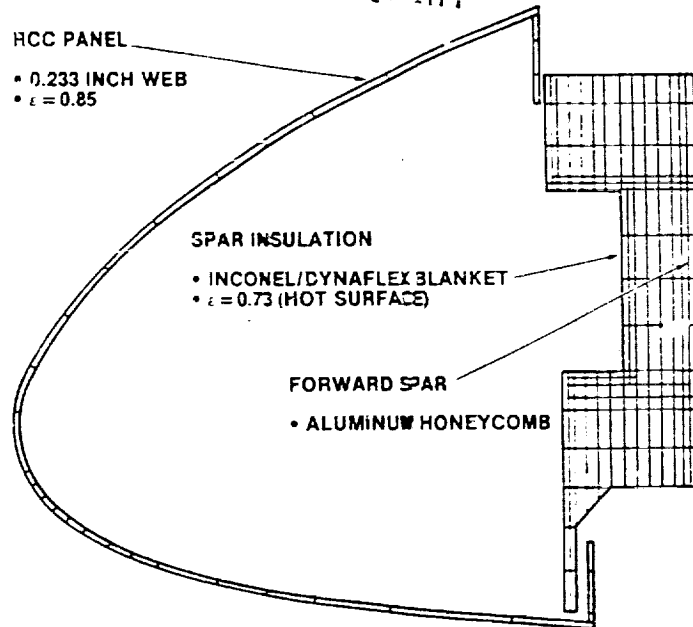


Figure 7.- Panel 61 RCC shell thermal math model.

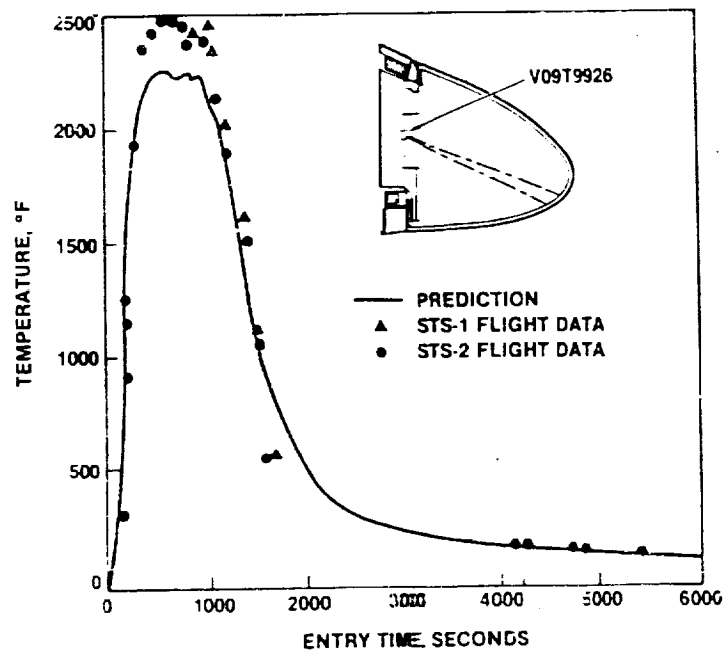


Figure 8.- Panel 9 radiometer T09T9926A data comparison to prediction.

ORIGINAL PAGE 15  
OF POOR QUALITY

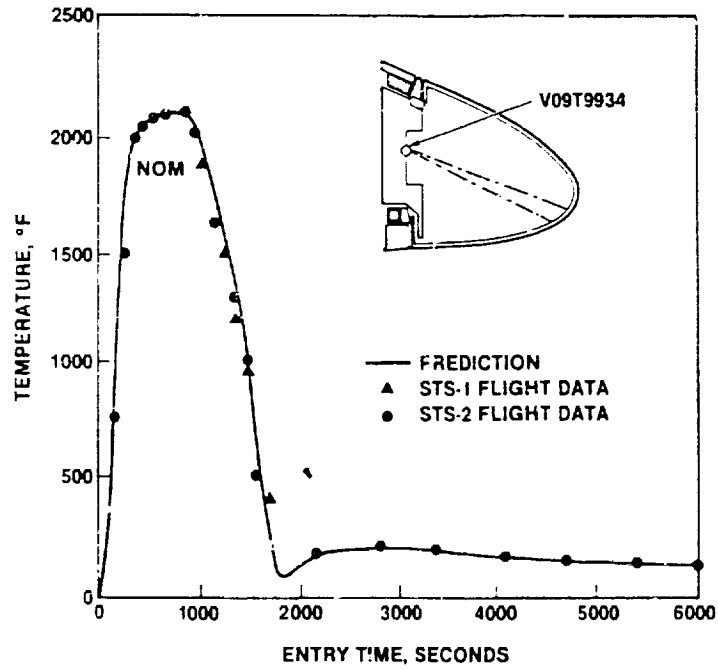


Figure 9.- Panel 16 radiometer V09T9934A data comparison to prediction.

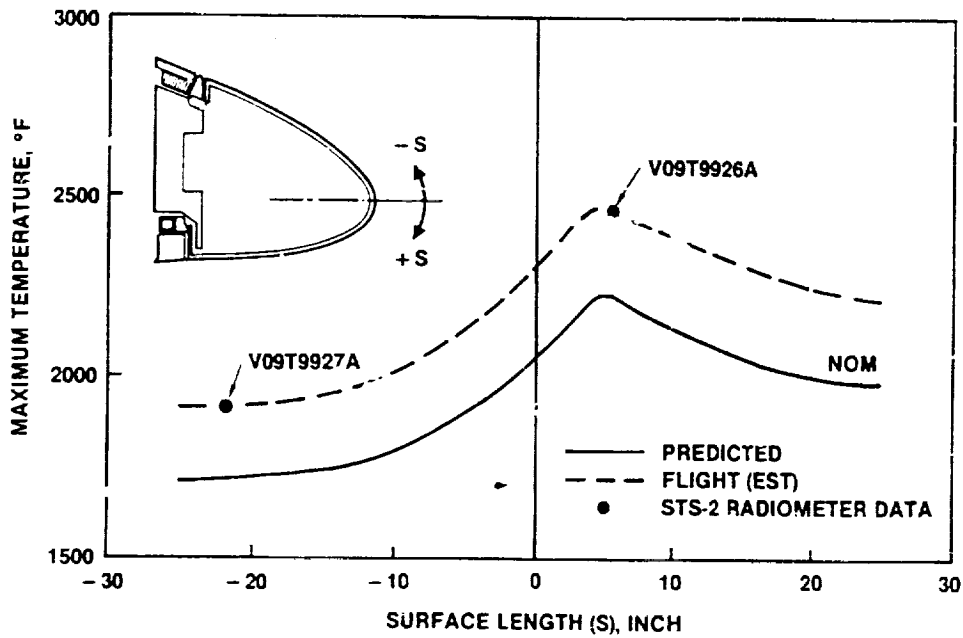


Figure 10.- Panel 9 temperature distribution.

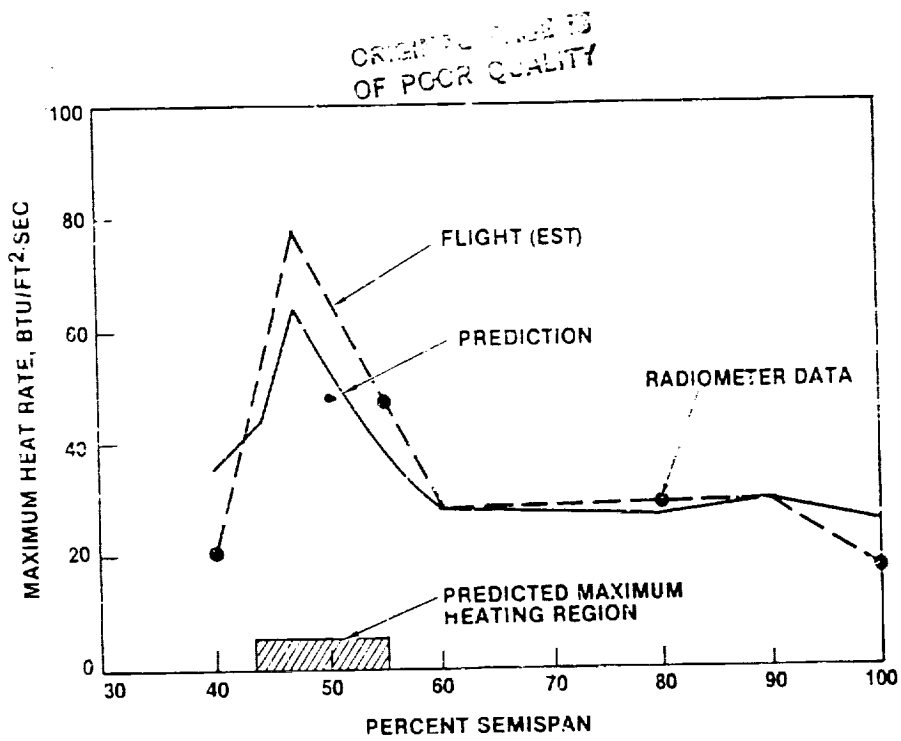


Figure 11.- Spanwise maximum heat rate comparison.

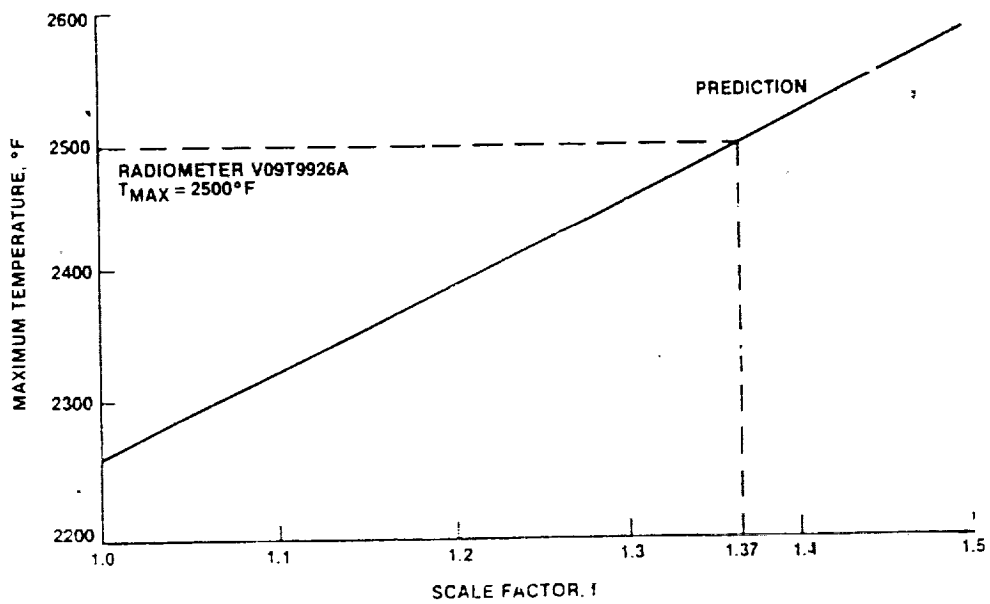


Figure 12.- Parametric scaling of predicted radiometer V09T9926A temperature.

ORIGINAL PAGE IS  
OF POOR QUALITY

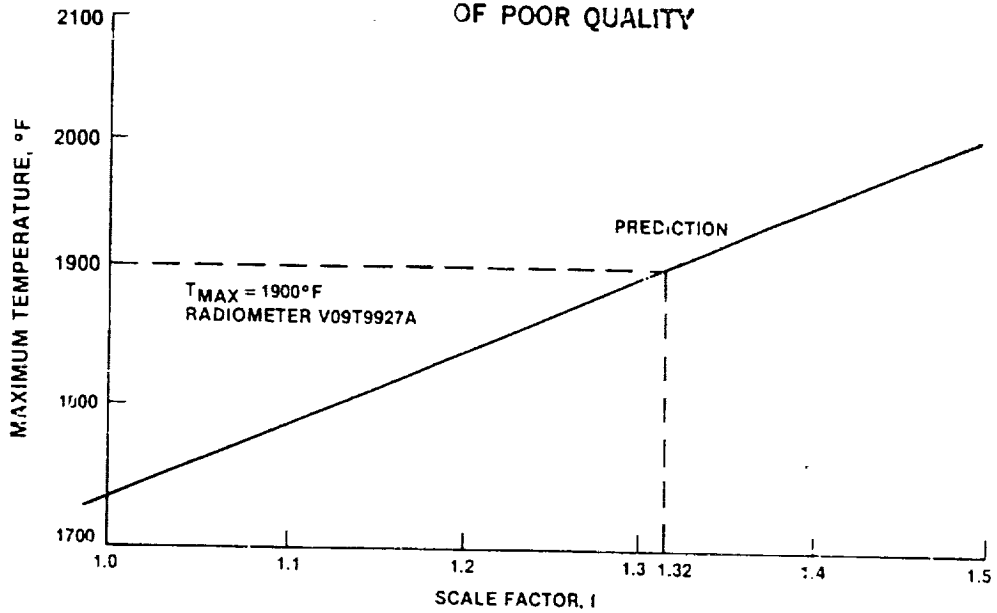


Figure 13.- Parametric scaling of predicted radiometer V09T9927A temperature.

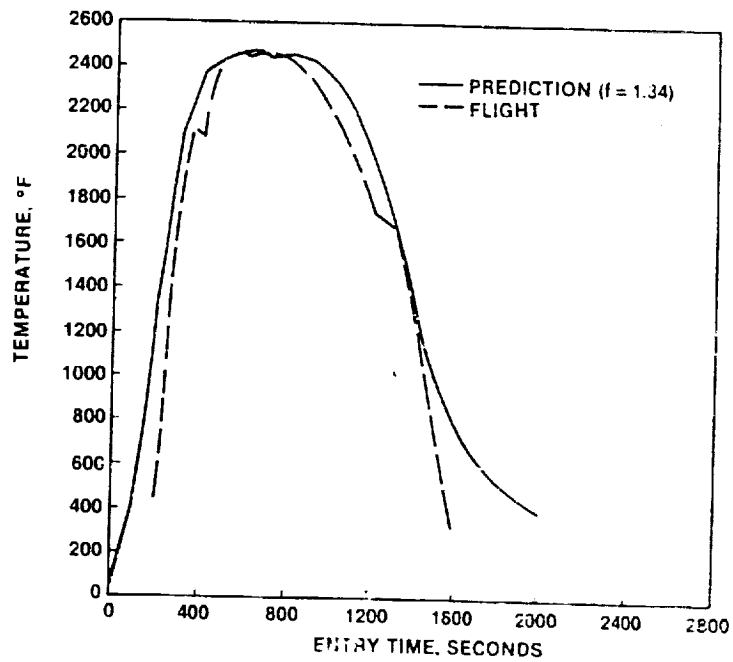


Figure 14.- Panel 9 maximum heating radiometer V09T9926A temperature prediction (f = 1.34).

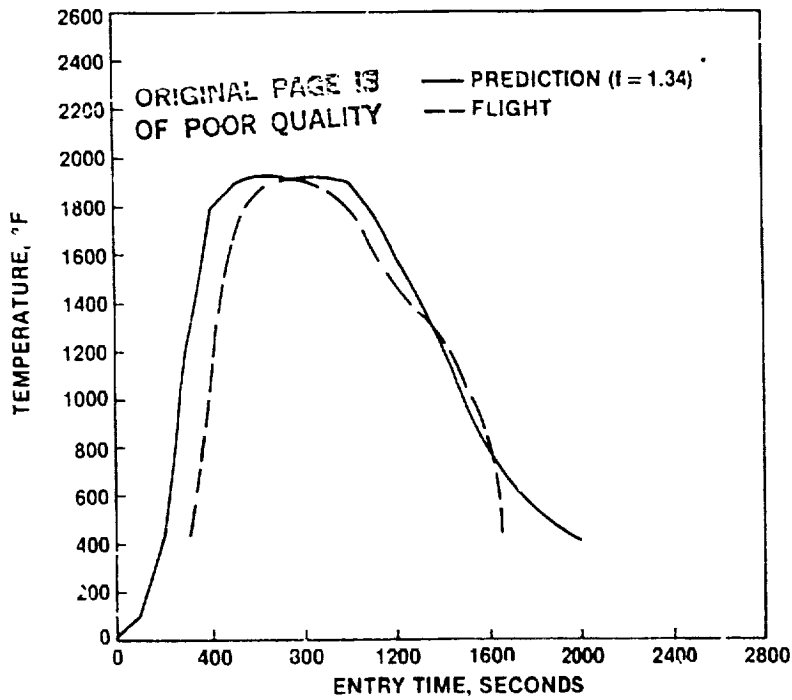


Figure 15.- Panel 9 leeward radiometer V09T9927A temperature prediction ( $f = 1.34$ ).

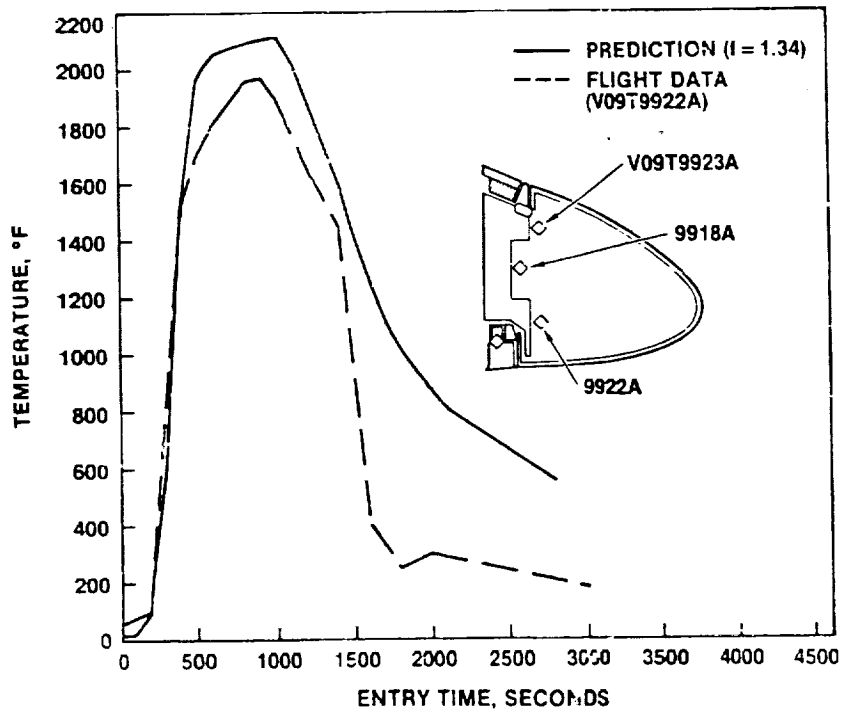


Figure 16.- Panel 9 lower insulation temperature prediction ( $f = 1.34$ ).

ORIGINAL PAGE IS  
OF POOR QUALITY

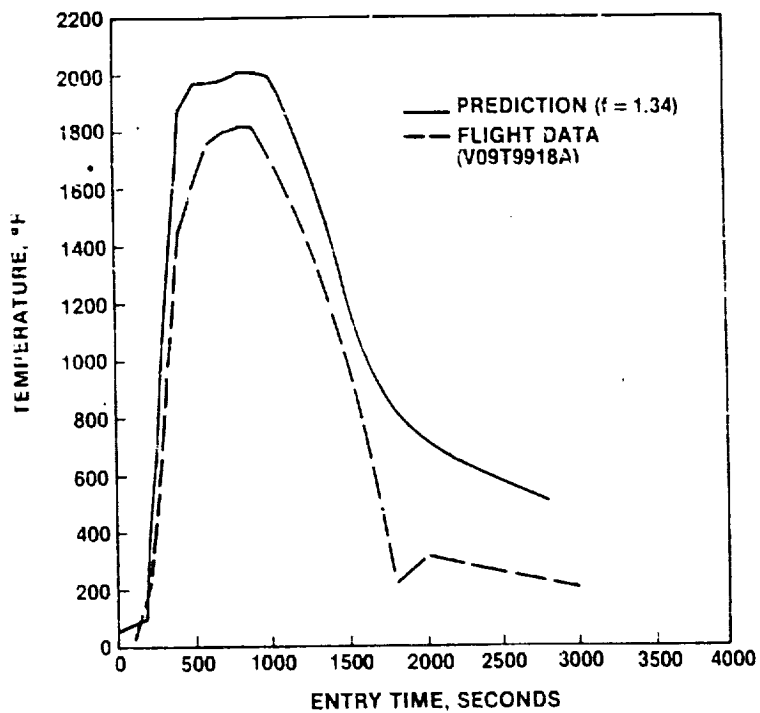


Figure 17.- Panel 9 insulation midplane temperature prediction ( $f = 1.34$ ).

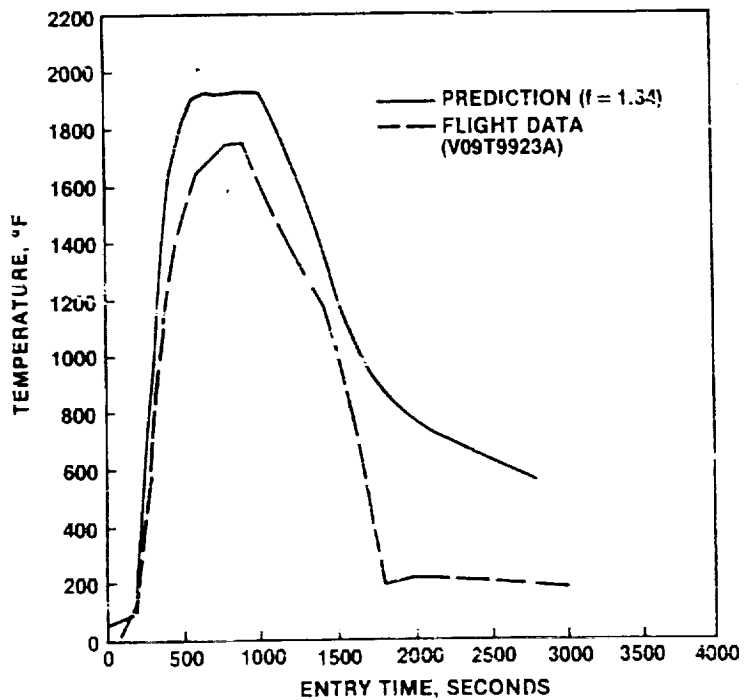


Figure 18.- Panel 9 insulation upper surface temperature prediction ( $f = 1.34$ ).

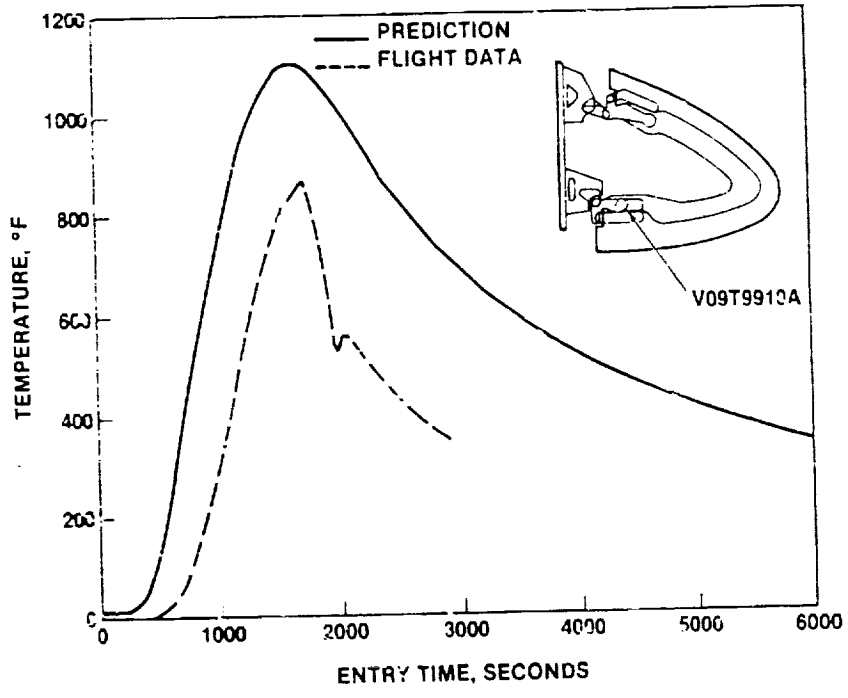


Figure 19.- Rib station 10 lower panel clevis temperature comparison ( $\bar{t} = 1.34$ ).

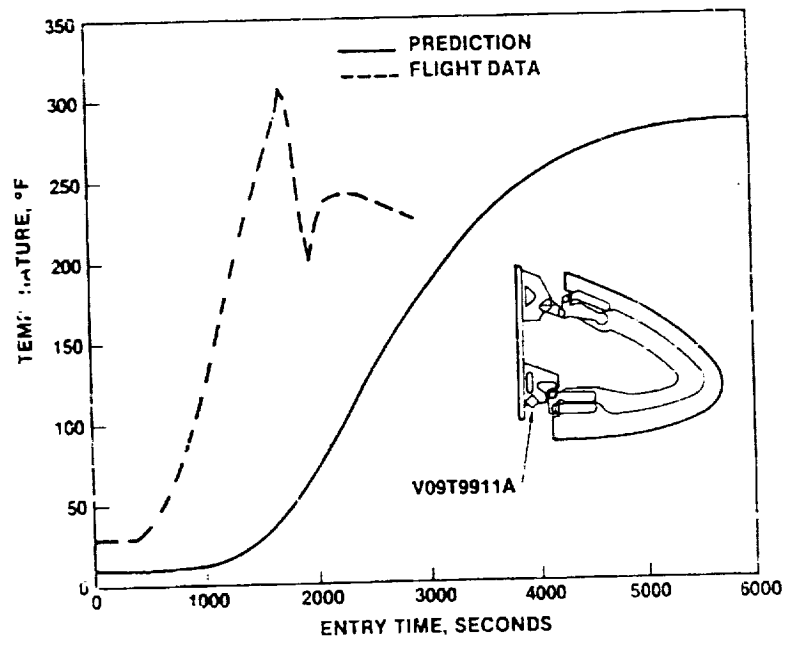


Figure 20.- Rib station 10 lower spar bracket temperature comparison.

ORIGINAL PAGE IS  
OF POOR QUALITY

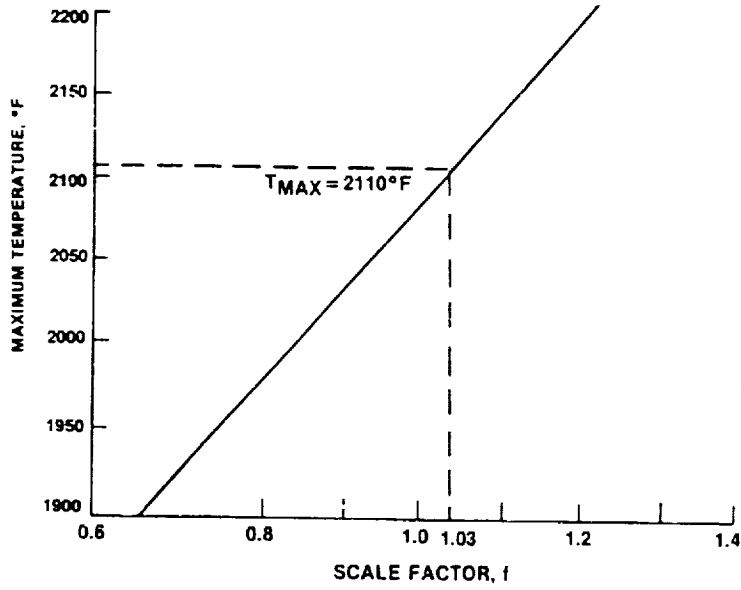


Figure 21.- Parametric scaling of predicted radiometer V09T9934A temperature.

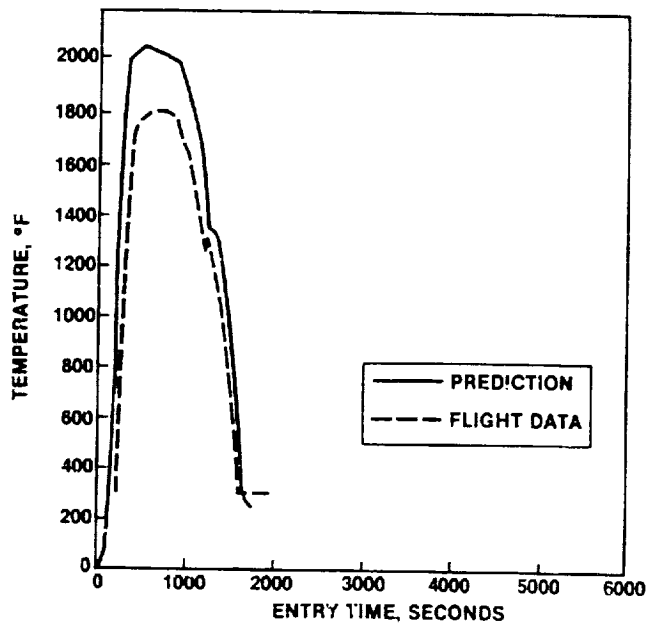


Figure 22.- Panel 4 radiometer V09T9909A data comparison to prediction.

ORIGINAL PAGE IS  
OF POOR QUALITY

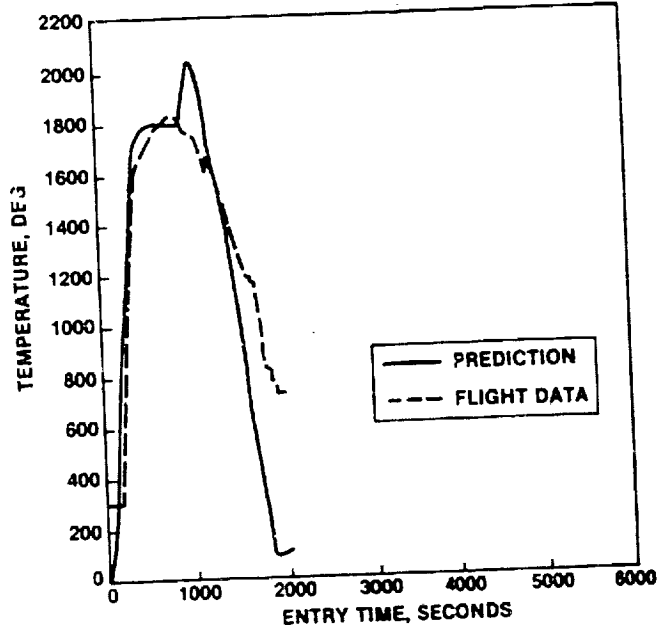


Figure 23.- Panel 22 radiometer V09T9940A data comparison to prediction.